Insight Generation from Information-Dense Formation Protocols

Leon Merker,* Bojing Zhang, Jun Yuan, Shanling Ji, and Helge Sören Stein*

Accelerated formation protocols that utilize pulsed charging offer an unprecedented wealth of electrochemical data. Herein, methods are presented to extract diagnostic data relating to pseudo-diffusion coefficients, internal resistance, and others that give live insight into solid electrolyte interphase (SEI) growth. Specifically, a purely mathematical method is used to track formation progression in near-real time and chart a path toward incorporation of adjustable pulse parameters for targeted SEI synthesis. The method and analysis are performed on 3 mAh cells but can also be applied to higher-capacity cells.

1. Introduction

Formation is a time-intensive production step,[1–3] predominantly performed by constant current constant voltage (CCCV) charging at charge rates (C-rates) well below, ranging from C/20 to C/15, that is, taking between 15 and 20 h. This rather slow charging can be accelerated using a pulsed protocol—not just for metallic anodes[4–7] but also for more industrially relevant graphite anodes.[8] Setting higher C-rates in CCCV formation to achieve faster formation is typically not advisable as it may cause lithium plating on the surface of the anode due to slow kinetics and even worsen further intercalation. Pulsed charging alleviates this shortcoming through bespoke tailoring of surface versus bulk diffusion. Furthermore, pulsed current formation is shown to lead to a more uniform and thinner solid electrolyte interface (SEI).[8,9] As demonstrated by the authors there is even the possibility to form cells at only 10 h without additional loss of Li-inventory compared to conventional constant current (CC) charging across a range of cell formats up to industrial relevant 25 Ah pouch cells.[10] The interesting electrochemical aspect of this protocol is the wealth of additional information of this highly dynamic system compared to conventional CC formation[1,11–13] and other formation strategies performing clever adjustment of the formation current and temperature.[11,12,14,15] The additional derivable parameters could be used to adapt or be combined with recent models predicting the quality and lifetime of batteries,[16–20] while reducing the amount of training data. Therefore, it may also reduce the number of costly experiments for research and industry. Analysis of this dynamic formation protocol does however necessitate a high data acquisition rate and resolution. Extraction of parameters is nontrivial as the pulses and rest times are within the second range as is typically found in longer and separate tests after formation, that is, in the galvanostatic intermittent titration technique (GITT). Today's high computational power does however enable the extraction, prediction, and optimization of live formation data even for individual cells and could lead to a new chapter of optimized formation on individual cell level.

This requires the adaptation of the pulse parameters during formation while maintaining safety, which is a challenge for industrial automation engineers and requires strong collaboration with electrochemists.

However, this method and the analysis is restricted by the data acquisition rate and the minimum toggle time of the current limited by the equipment.

This publication presents the determination of a set of selected parameters from incremental capacity analysis (ICA),

L. Merker
Helmholtz Institute Ulm
Helmholtzstr. 11, 89081 Ulm, Germany
E-mail: leon.merker@tum.de

L. Merker
Karlsruhe Institute of Technology
76021 Karlsruhe, Germany

L. Merker, B. Zhang, J. Yuan, S. Ji, H. S. Stein
Technical University of Munich
Lichtenbergstr. 4, 85748 Garching, Germany
E-mail: helge.stein@tum.de

L. Merker, B. Zhang, J. Yuan, S. Ji, H. S. Stein
Department of Chemistry
Chair of Digital Catalysis
TUM School of Natural Sciences
Lichtenbergstraße 4, 85748 Garching, Germany

L. Merker, B. Zhang, J. Yuan, S. Ji, H. S. Stein
Munich Institute of Robotics and Machine Intelligence (MIRMI)
Georg-Brauchle-Ring 60, 80992 Munich, Germany

L. Merker, B. Zhang, J. Yuan, S. Ji, H. S. Stein
Munich Data Science Institute (MDSI)
Walther-von-Dyck-Str. 10, 85748 Garching, Germany

L. Merker, B. Zhang, J. Yuan, S. Ji, H. S. Stein
Munich Institute of Integrated Materials
Energy and Process Engineering (MEP)
Lichtenbergstr. 4 a, 85748 Garching, Germany

L. Merker, B. Zhang, J. Yuan, S. Ji, H. S. Stein
Munich Center for Machine Learning (MCML)
Oettingenstraße 67, 80538 Munich, Germany

Batteries & Supercaps

Research Article
doi.org/10.1002/batt.202500153

**Chemistry
Europe**
European Chemical
Societies Publishing

hybrid pulse power characterization (HPPC) and the GITT of pulsed formation data. The extracted parameters of dQ/dV, internal resistance (IR) and a pseudodiffusion coefficient are presented, evaluated, and compared along the progression of the formation process.

2. Experimental Section

Detailed specifications of the materials used, as well as the assembly and test procedure correspond to the ones published by the authors in Ref. [10] and are only summarized here. Focus of this publication is the analysis and parameter extraction of the pulsed formation.

Coin cells were automatically assembled by the AutoBASS system in a nitrogen containing glovebox. The cells contain 14 mm discs of NMC (622) cathodes, 15 mm discs of graphite anodes, 16 mm discs of Celgard 2325 separator (25 μm microporous trilayer membrane (polypropylene/polyethylene/polypropylene)), and 35 μL of 1 M $LiPF_6$ in EC:EMC (3:7 wt:wt) electrolyte from the manufacturer E-Lyte. The nominal capacity c_{nom} for all cells was calculated to be 3.28 mAh based on the areal cathode discharge capacity of 2.14 mAh cm^2 at 1C discharge given by the supplier ZSW. Within the formation process used pulses, a current I_{pulse} was applied for a defined time t_{on} to V_{top} followed by a rest step lasting t_{off} to V_{bot} summing up to the pulse length t_{pulse}. This pulse was repeated until V_{limit} of 4.2 V was reached.

The transient voltage of the formation charge and an exemplary pulse are depicted in **Figure 1**. The maximum voltage of the pulses V_{top} and minimum voltage during rest V_{bot} are used for the following dQ/dV, IR and a pseudodiffusion coefficient analysis of the formation.

The pulsed formation experiments are clustered in two subsets of acceleration with effective C-rates of C/8.2 and C/7.2, including different variations of the pulse parameters (I_{pulse}, t_{on}, t_{off}, and t_{pulse}). Changes were made to a "reference" pulse of 4.33 s (t_{on} = 3 s, t_{off} = 1.33 s) and C/5.7 current and are indicated by their names. The reference pulse parameters were derived from an internal master thesis investigating pulse parameters to minimize lithium plating during charging.

For comparison, a CC formation with C/8.2 was performed. After formation an end-of-line test (EOL) was performed including measurement of the IR and self-discharge. For all cells, long-term stability tests were performed after EOL test using 1 C CCCV until C/20 was reached in the CV step for charging and 1 C CC discharge for 300 cycles. Further information can be found in Ref. [10] and the Supporting Information.

2.1. ICA

The ICA commonly investigates the change of capacity with changing voltage in dQ/dV plots.

In pulsed formation there need to be some adjustments to this technique. For the determination of dQ/dV the formation charge value Q was calculated by the pulse current i_{pulse} multiplied with the respective time the current flowed t_{on} during the pulse.

$$Q = i_{pulse} \cdot t_{on} \tag{1}$$

The calculation of the voltage difference dV for each pulse was carried out using either the end voltages V_{top} of the charge phase of the pulse or the end voltages V_{bot} of the rest phase.

As the high data acquisition rate for pulses resulted in comparably small inaccuracies in pulse timing, linear regression of the pulse voltages during charge was performed to enable comparison of voltages at specific times within the pulse.

Voltage and dQ/dV values were smoothed using scipy's implementation of the Savitzky–Golay–Filter.

For the formation discharge the charge value Q was calculated equivalently to (Equation 1) using the discharge current $i_{discharge}$ and the elapsed time. The authors were aware of the possibility of capacity changes during the rest phase that could not be detected here but in a three-electrode setup. These changes were assumed to be a neglible, also due to the short rest time.

2.2. IR

For the determination of the IR R_i, every charge pulse of the formation was interpreted as one HPPC experiment, and Ohm's law was used to calculate the resistance. As denominator the value of the charge current i_{pulse} and as numerator the voltage difference between the bot voltage V_{bot} and the top voltage V_{top} were utilized.

$$R_i = \frac{\Delta V}{i} = \frac{V_{top} - V_{bot}}{i_{pulse}} \tag{2}$$
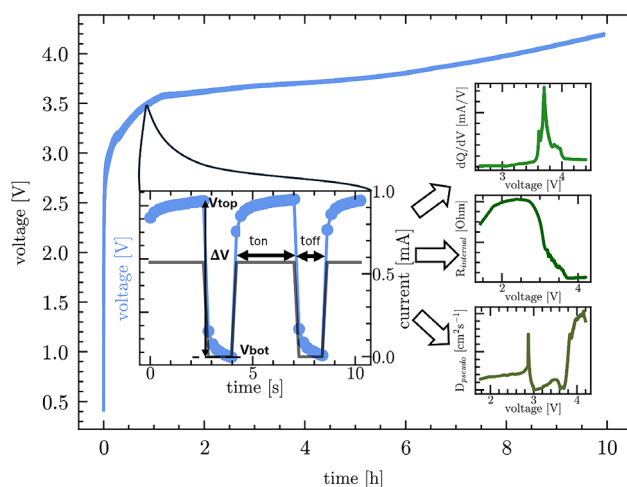

Figure 1. Emblematic formation voltage transient using C/5.7 pulses (t_{on} = 3 s, t_{off} = 1.33 s, and current i = C/5.7). For the formation pulses, a current I_{pulse} was applied for a defined time t_{on} increasing the voltage to V_{top} followed by a rest step lasting t_{off} relaxing the voltage to V_{bot} as indicated in the inset. The measured values are then used to perform dQ/dV, IR, and a pseudodiffusion coefficient analysis over the entire formation process.

Batteries & Supercaps

Research Article
doi.org/10.1002/batt.202500153

Chemistry Europe
European Chemical
Societies Publishing

2.3. Diffusion Coefficient

Each pulse can be seen as a very fast GITT experiment and therefore enables the determination of the chemical diffusion coefficient D_{chem} by the formulas proposed by Weppner and Huggins.[8] The chemical diffusion coefficient can be calculated by

$$D_{chem} = \frac{4}{\pi} \cdot \left(\frac{V_{mol}I_0}{SF}\right)^2 \cdot \left(\frac{\frac{dE}{d\delta}}{\frac{dE}{d\sqrt{t}}}\right)^2 \quad (t \ll L^2/D) \tag{3}$$

where I_0 (A) is the current of the charge pulse, V_{mol} (cm^3 mol^{-1}) the molar volume of the electrode, S (cm^2) the surface area of the electrode, and F (C mol^{-1}) the Faraday constant.

$dE/d\sqrt{t}$ is the slope of the pulse potential transient in the linearized representation. The equation is valid for pulse times t_{pulse}, being way lower than the squared electrode thickness L divided by the diffusion coefficient.

$dE/d\delta$ is change of the steady-state voltage E with the stoichiometry δ of lithium in the electrode. The change in stoichiometry is estimated to be constant for such short pulses.

3. Results and Discussion

3.1. ICA

For the formation and cycling an ICA with resulting dQ/dV plots was performed and results are presented in **Figure 2**.

The determined dQ/dV values were plotted over the respective voltage V_{top} for the charge and discharge for one cell of each pulsed formation. The red curves illustrate the formation, whereas the other curves display the resulting dQ/dV plots of 1 C charge and discharge cycling every 50 cycles up to 300. For the reference CC C/8.2 formation as well as the cycling results the dQ/dV values are plotted over their respective measured voltage.

For all formation curves two peaks and one shoulder for the charge curve, as well as one peak for the discharge curve can be identified. The dQ/dV cycle curves show only two peaks for charge and one for discharge and decreasing values throughout all curves with increasing cycle number. The increased C-rate of the cycling compared to the formation should shift peaks to higher voltages for charging[21–23] and lower voltages while discharging. Latter effect is observable in the plots but no clear and consistent increase for peaks in the charge part can be seen.

Table 1 presents the average voltage peaks and underlying structural changes of NMC according to and in agreement with literature.[9–12] The first peak while charging refers to the lithiation of graphite $C_6 \rightarrow LiC_x$, whereas the second peak refers to the transition of NMC from rhombohedral to monoclinic and further lithiation of graphite. The following smaller shoulder around 3.9 V is assigned to the transition of NMC from monoclinic to rhombohedral. This peak loses intensity and is shifted to higher potentials with increased cycle number in agreement with.[6] Only in the formation of the CC C/8.2 cells a small peak around 3.2 V can be identified that could refer to a formation reaction. Increasing and nonzero values hint toward already ongoing reactions which can be assigned to formation reactions[24] and electrolyte decomposition.[12] The additional peak around 4.1 V, observable only at the CC C/8.2 pulsed mixed C/5.7 + C/20 curves could not be assigned.

For the discharge only one peak throughout all formation strategies could be identified. The discharge peaks represent
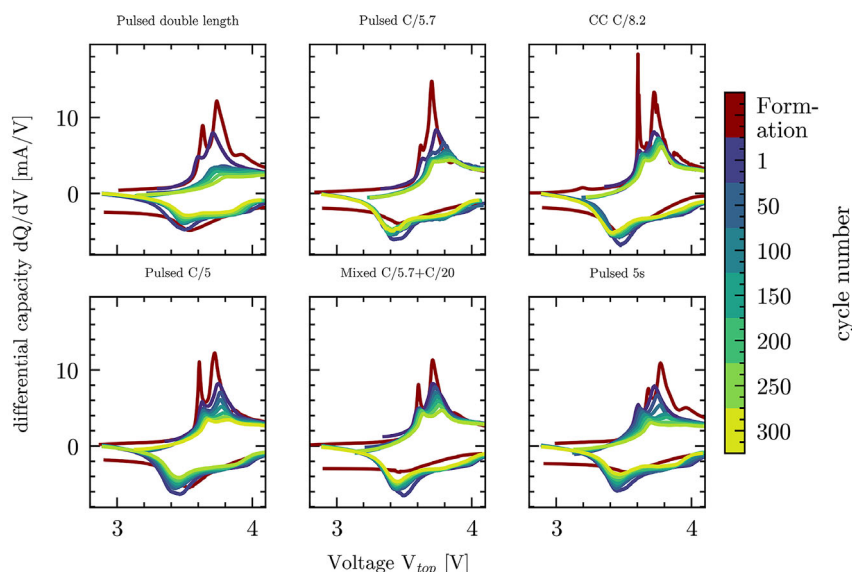

Figure 2. Extracted dQ/dV plotted over the end voltage V_{top} of the respective pulse for the formation and the voltage measured for the CC C/8.2 cell. The red curves represent the results of the formation analysis, whereas the curves with increasing lightness display the results of every 50th 1C charge and discharge cycle. For all formation curves two peaks and one shoulder for the charge curve, as well as one peak for the discharge curve can be identified. The 1C cycle curves show only two peaks for charge and one for discharge and decreasing values throughout all curves with increasing cycle number. The increased C-rate of the cycling compared to the formation shift peaks to higher voltages for charging[21–23] and lower voltages while discharging.

Batteries & Supercaps

Research Article
doi.org/10.1002/batt.202500153

Chemistry
Europe
European Chemical
Societies Publishing

Table 1. Summarizes the assignment of observed dQ/dV peaks of one cell to underlying reactions and effects.

Strategy[a]	Lithiation $C_6 \rightarrow LiC_x$	H1 → M (rhombohedral to monoclinic) + Lithiation	M → H2 (monoclinic to rhombohedral)	Additional	Discharge peak
Pulsed double length	3.63 [V]	3.73 [V]	3.91 [V]		3.48 [V]
Pulsed C/57	3.62 [V]	3.72 [V]	3.88 [V]		3.46 [V]
CC C/8.2	3.60 [V]	3.72 [V]	3.90 [V]	3.20 [V] 4.11 [V]	3.46 [V]
Pulsed C/5	3.60 [V]	3.72 [V]	3.89 [V]		3.50 [V]
Mixed C/5.7 + C/20	3.61 [V]	3.73 [V]	3.88 [V]	4.16 [V]	3.50 [V]
Pulsed 5s	3.65 [V]	3.74 [V]	3.94 [V]		3.50 [V]

[a]The first peak around 3.6 V can be assigned to the lithiation of graphite, the second one to the transition of NMC from rhombohedral to monoclinic and further lithiation of graphite. The shoulder around 3.9 V is assigned to the transition of NMC from monoclinic to rhombohedral. The additional peak around 3.2 V of CC C/8.2 is assumed to be originating in formation processes, whereas the peak at around 4.1 V for the CC C/82. and mixed pulsed C/5.7 + C/20 cell could not be assigned or explained. The discharge peak represents the inverse reactions and transitions of the charge curve and is assumed to represent the delithiation of graphite. Other reverse reactions can not clearly be identified as a result of increased C-rate and data resolution.

the inverse reactions and transitions of the charge curve, but only one peak is observable most likely due to lower data acquisition rate and therefore lower resolution. The discharge peak is assumed to be the delithiation of graphite. The peaks' intensity and width of all pulsed formed cells is in the same range, where in contrast the CC C/8.2 cells have sharper and higher intensity peaks in the charge curve. The broadening could be a consequence of relaxation time of the pulse leading to smaller voltage differences and the resulting increased influence of the necessary smoothing. To investigate the influence of the chosen data point of pulse for the determination of dQ/dV was performed using the differences of V_{top} values and V_{bot} values of every pulse for the calculation. The resulting plots of all strategies and cells can be found in Figure S4 and S5, Supporting Information, and only minor differences can be identified.

It has to be mentioned that the high data acquisition rate during the charge pulses results in various numbers of data points and smaller differences in time from pulse to pulse.

Linear extrapolation was used on all pulses to ensure a consistent number of 16 data points at fixed times and again dV was calculated by the difference of the first voltage of the pulse to the first voltage of the subsequent pulse. The plots were chosen to be separated by an increasing value to enable distinguishment, as shape and intensities of all curves show nearly the same values. The resulting waterfall plot can be found in **Figure 3**.

These plots show that the voltage increases during the charge part of the pulse and the underlying effects of polarization and resistance are nearly indistinguishable for short the pulses.

3.2. IR Analysis

Figure 4 presents the determined IR of the formation of all strategies plotted over the respective top voltage V_{top} of the pulses.

The IR was calculated by interpreting every charge pulse as a small HPPC experiment and using Ohm's law to calculate the resistance. Note here that the mixed C/5.7 + C/20 cells are excluded, as during t_{off} a smaller current is applied, and therefore the resistance calculation is not applicable.
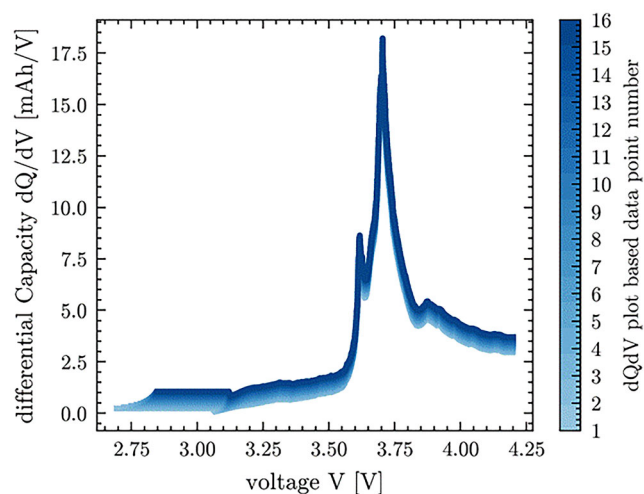

Figure 3. Differential capacity dQ/dV plots of linear extrapolated pulses. Pulse data was extrapolated to a consistent number of 16 data points at fixed times. For the calculation of dV the voltage difference of subsequent pulses was performed using the same data point (1–16) of the extrapolated pulse. Plots were stacked on top of each other. These results hint toward the constant polarization and resistance throughout the pulse.

For all curves a rising resistance from a high starting value, followed by a decrease to a consistent end value at higher voltages can be observed.

The study of peak maxima reveals the highest maxima for the doubled pulse length formation as well as the lowest maxima for the pulsed C/5 formation. The increased time of rest and relaxation of the doubled length leads to lower voltages up to the open-circuit potentials (OCP) and consequently due to the Ohm's law dependency to higher resistances. The lower maxima for the C/5 formation can also be explained by shorter relaxation times, lower voltage differences, and the inverse dependenc of resistance on current. Despite having the same effective C-rate, the pulsed 5s cells show higher values due to the lower current and same relaxation time.

Table 2 summarizes the values for maxima and minima resistances and their respective voltages, as well as a determined IR

Batteries & Supercaps

Research Article
doi.org/10.1002/batt.202500153

Chemistry
Europe
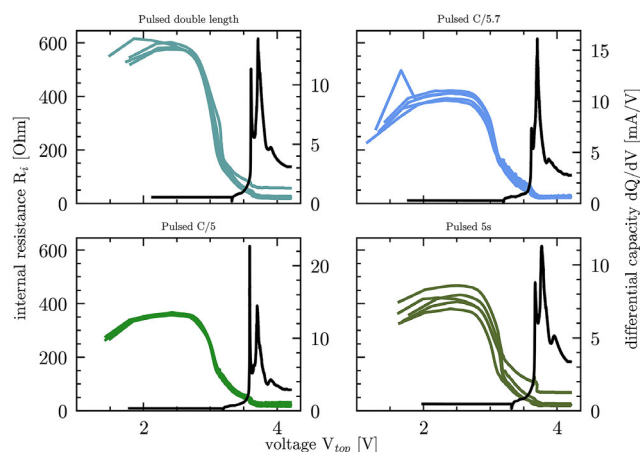
European Chemical
Societies Publishing

Figure 4. IR by HPPC plotted over the end voltage V_{top} of the respective pulse. For all curves a rising resistance from a high starting value, followed by a decrease to a consistent end value at higher voltages can be observed. The study of peak maxima reveals an increased maxima of the pulsed formation with doubled pulse length as well as the lowered maxima of the pulsed C/5 formation, explainable by Ohm's law.

value after the formation. This value was determined after two additional cycles (see EOL in Supporting Information) using HPPC at a cell voltage of 4 V and a 3 C discharge current. For comparison reasons the IR values at 4 V of the formation strategies were averaged excluding outliers denoted in brackets. The IR values determined during formation and EOL are within the same range, where differences can be explained by the high current used in the measurement during EOL and the used pulse of discharge during EOL, whereas the charge pulse is used in the formation.

To the best of our knowledge there is no existing data of continuously measuring IR during the formation especially in that time interval. The course can therefore only be compared to resistance measurements directly following the formation.

Comparing the transient within the batteries working voltage window (2.9–4.2 V) the decrease with rising voltage to a threshold value can also be seen in other publications.[25–27]

To the best of the author's knowledge, there are no publications investigating the IR at low voltages and no explanation was found for the observed shoulder in the plots. The authors assume a connection to the rapidly increasing voltage when applying

current to a freshly assembled cells until some voltage, but further investigations are needed.

3.3. Diffusion Coefficient

For the diffusion coefficient in (Equation 3), the slope of the partial derivatives $dE/d\delta$ and $dE/\sqrt{t}$ are the most informative parameters and can be extracted independently of the cell geometry. The determination of $dE/\sqrt{t}$ is derived conventionally by fitting the voltages V_{top} over the respective time to a square root function to calculate the slope.

$$E(t) = A \cdot \sqrt{t} + B \tag{4}$$

The coefficient of determination R^2 is used as the primary indicator for the quality of fits. The determination of $dE/d\delta$ and $dE/d\sqrt{t}$ in the following section is performed for one cell of C/5.7 pulsed formation. **Figure 5**a shows values of R^2 close to 1 up to 2 V for the square root fit, followed by a decrease down to 0.77 at 3.2 V, and start rising back over 0.9 around 3.7 V. Larger scattering can be observed at higher voltages(>3 V) and can be explained by the limited resolution of the cycler and only small voltage differences during phase transitions in this voltage region. The voltage region of lower coefficients matches the region of phase transitions identified in the dQ/dV plots and the square root dependance indicate toward diffusion-based process, also in the transition region.

The phase transition and reactions are estimated to be of kinetic first order and can be described by the following exponential function

$$E(t) = A \cdot \exp(-B \cdot t) + C \tag{5}$$

Using the sum of both functions as the fit function shows improved R^2 values and less scattering at higher voltages. The combined fit describes the relation between voltage response of the pulse and time via

$$E(t) = A \cdot \exp(-B \cdot t) + C \cdot \sqrt{t} + D \tag{6}$$

The sum of A and D correspond to the starting voltage of the pulse at $t = 0$ when applied to each pulse. In Figure 5b, the starting voltages of the pulses are plotted for both fit functions and

Table 2. Summary of the averaged maxima and minima of the determined IR and their respective averaged voltage.

Strategy	Average maxima [Ohm]	Average voltage [V]	Average minima [Ohm]	Average voltage [V]	Avg IR form @4 V [Ohm]	IR EOL @4 V [Ohm][a]
Pulsed double length	591	2.29	30	4.03	24 (58)	≈16
Pulsed C/57	421	2.22	23	3.76	25	≈20
Pulsed C/5	362	2.40	21	4.01	22	≈16
Pulsed 5s	422	2.43	30	4.03	22(68)	≈16

[a]Furthermore, it presents the values of the average IR of the formation at 4 V, as well as the resistance similarly measured and determined in the later performed EOL test. The values in round brackets are considered outliers. As part of the EOL, the IR is determined by HPPC but using a 3C discharge pulse in contrast to the charge pulse used for the formation. To the best of our knowledge there is no existing data of constantly measured IR during the formation but agrees in the range of 2.9–4.2 V with other publications.[25–27]
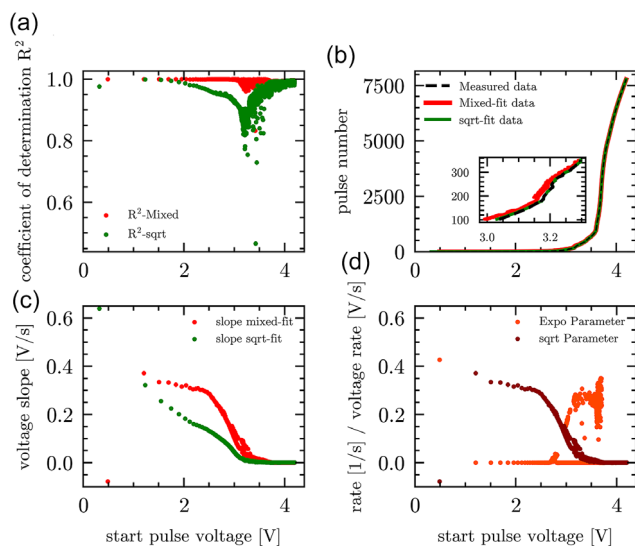
Batteries & Supercaps

Research Article
doi.org/10.1002/batt.202500153

Chemistry Europe
European Chemical
Societies Publishing

Figure 5. a) Coefficient of determination R^2 of one cell using pulsed C/5.7 formation ($t_{on} = 3$ s, $t_{off} = 1.33$ s, and current $i = C/5.7$). The square root fit represents the curve well up to 2 V and after 3.7 V, decreasing down to 0.77 at 3.2 V. Larger scattering can be observed at higher voltages (>3 V). b) Extracted starting voltages for every pulse of the square root fit, the mixed fit and the measured data. c) Parameter C of the square root fit, as well as the mixed fit plotted over the starting pulse voltage. This parameter determines the slope of $dE/d\sqrt{t}$ and higher values can be observed for the mixed fit slopes throughout the region of lower R^2 square root fits. d) Comparison of of parameter C (square root parameter) and B (expo parameter) plotted over the respective starting voltages of the pulse.
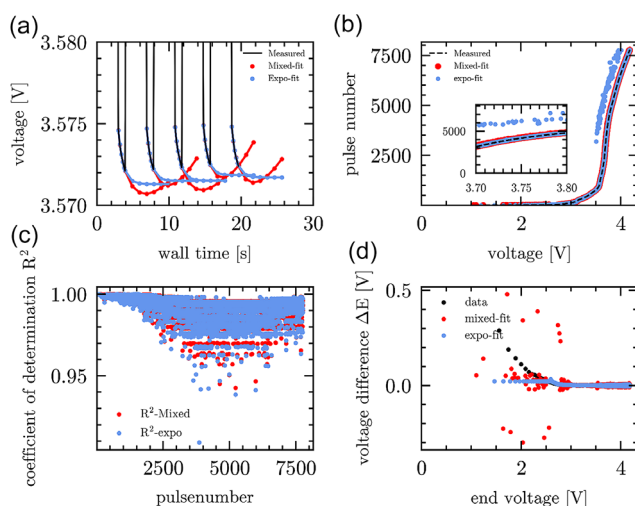

Figure 6. a) Example of the voltage transient plotted over of pulse time of the formation using C/5.7 ($t_{on} = 3$ s, $t_{off} = 1.33$ s, and current $i = C/5.7$). The data of the pulses rest time was fitted to an exponential function described in (Equation 5) and another mixed function of square root and exponential described in (Equation 6). The fits are used to estimate the OCP as the rest time is too short for the system to fully relax. b) Starting voltage values calculated by the sum of parameters A and D for the mixed fit, and as the sum of A and C for the exponential function plotted against the pulse number. The transient of the exponential fit and mixed fit matches the measured data throughout the curve. c) Comparison of the exponential and the mixed fit. d) Calculated difference of the limiting voltages C for the exponential, difference of minima estimated by the mixed fit and differences of the measured minima voltages at the end of the rest time for each pulse.

the measured data. All curves are nearly indistinguishable at higher voltages but the mixed fit shows lower values in the region of 2.7–3.3 V presented in the zoomed-in plot. Even though the R^2 for the square root fit is low in this voltage range, the voltage values nearly match the measured ones.

These starting voltages were also used to determine dQ/dV values for both fits and are plotted against the starting voltage in Figure S6, Supporting Information. The curves show the same peaks and shape, in agreement with plots in Figure 2.

The slope of $dE/d\sqrt{t}$ can be directly extracted from the fit parameter A of the square root fit and from parameter C of the mixed fit, where contributions of the exponential function in parameter A are found to be negligibly low. Figure 5c presents the $dE/d\sqrt{t}$ slopes of the pulses over the respective first voltage of the pulse. Higher values can be observed for the mixed fit slopes throughout the region of the phase transition. Conspicuously the first slope value of the mixed fit is slightly negative, whereas the square root fit value has its maximum value but no explanation was found.

In Figure 5d, the exponential parameter B and square root parameter C of the mixed fit function of each pulse are plotted over the respective first pulse voltage. These parameters allow conclusions to be drawn about the reaction rate of diffusion(C) and reactions of the phase transition(B). The initially elevated high value of B indicates reactions and high reaction rates and potentially associated with SEI from SEI formation reactions. Higher values of B are also observed in the voltage region around 3.5 V, where phase transition and other reactions previously have been linked to. In contrast, the square root parameter C exhibits decreasing values matching the decreasing speed of diffusion and intercalation at higher voltages.

$dE/d\delta$ describes the change of voltage with the change of stoichiometry of lithium in the electrode. The change of stoichiometry $d\delta$ is estimated to be constant throughout the voltage range and therefore negligible. The voltage change dE from pulse to pulse can be determined by the difference of open-circuit voltage (OCV) of the relaxed system. The authors are aware that the lithium loss as a result of formation reactions will not change the stoichiometry but assume the change due to the shortness of the used pulses as negligible.

There are ongoing discussions and a wide range of used rest times[28,29] within the pulses of GITT measurements to ensure a fully relaxed system.

As the rest time of a few seconds used within this article is clearly below common times, the OCV is estimated by a fit.

As fitting approaches, the mixed function of (Equation 6) and the exponential function of (Equation 5) were employed. **Figure 6**a presents the voltage transient of exemplary pulses of the C/5.7 formation and the corresponding fit courses of the voltage during rest time. By design the mixed function does not possess a natural asymptotic voltage limit at infinite time due to the square root function. Consequently, the minimum of the fitted voltage curve—including extrapolated values—is used to approximate the OCV for each pulse. The exponential fit has its limit value described by the C parameter. For both fits the

Batteries & Supercaps

Research Article
doi.org/10.1002/batt.202500153

Chemistry Europe
European Chemical
Societies Publishing

starting voltage of the pulse at $t = 0$ was identified to be the sum of parameter A and D for the mixed and A and C for the exponential fit. Measured values for the starting voltage of the rest time and the resulting values for both fits are plotted in Figure 6b. The general transient of the exponential fit and the mixed fit matches the measured values but for higher voltages scattering can be observed for the exponential fit values. Investigation of the associated pulses reveals a reasonable fit but a steeper voltage transient than seen in previous pulses and therefore lower voltages. No explanation for this behavior was found but reduce the influence of the exponential fit curve was smoothed.

The coefficient of determination presented in c is high and similar for both fits over the pulse number but also scattered and decreasing in the phase transition range (4000–6000 pulses equal the range of 3.75–4.0 V).

In Figure 6d, the voltage difference ΔE of the last measured voltage of the data, the difference of minima voltage estimated by the mixed fit and the difference of limiting voltage of the exponential fit are plotted. Voltage difference of the exponential fit is determined lower in the beginning but approaches the differences of measured data around 3 V. For the mixed fit differences larger scattering can be observed throughout the values and the exponential values are therefore chosen for further calculations.

The evolution of the rate parameter B in Figure S7, Supporting Information, shows positive numbers and a peak around 3.2 V with larger scattering afterward. Comparing absolute numbers to the charge rate parameter in Figure 5d this would hint toward even more reactions happening during the rest time, but more investigations are needed.

The previously determined parameters for the calculation of the diffusion coefficient using (Equation 3) are unconventional due to the shortness of the pulses and the boundaries of the equation of Weppner and Huggins.[8] To distinguish the resulting values from standard diffusion coefficients and avoid misinterpretation, the authors refer to them as pseudodiffusion coefficient. The authors suggest to use this parameter as qualitative indicator and focus on analysing trends rather than the actual values.

Figure 7a presents the determined pseudodiffusion coefficient for one cell using the C/.57 formation calculated by (Equation 3) using the previously calculated values of voltage difference ΔE as $dE/d\delta$ and the slope of $dE/d\sqrt{t}$. V_{mol} is determined by division of the molar mass of graphite by its density. The contact area is estimated to be the area of the anode which is calculated to be 1.77 cm². Values are plotted against the last voltage of the respective pulse.

The previously visible scattering of the slope of $dE/d\sqrt{t}$ and the voltage difference ΔE especially at potentials >3.7 V is even further increasing the values due to their potentiation in the calculation.

Therefore, the authors decided to discard all data that is within the top 25% of highest calculated values, resulting in the retention of ≈ 90% of total data.
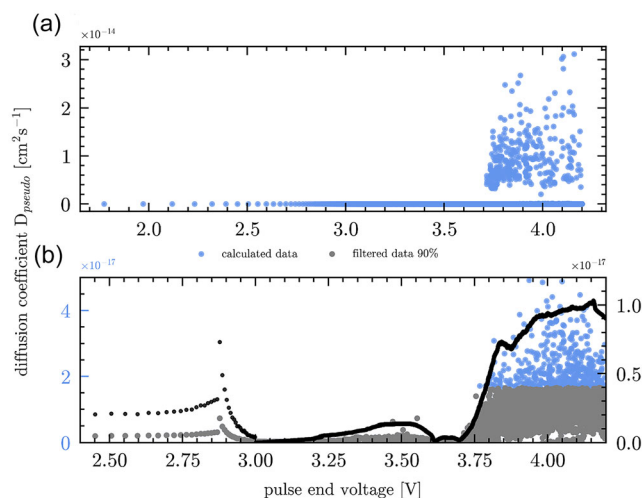

Figure 7. a) Pseudodiffusion coefficient for one cell using the C/.57 formation and the previously calculated values ΔE and $dE/d\sqrt{t}$. Values are plotted against the last voltage of the respective pulse. The scattering of $dE/d\sqrt{t}$ and ΔE and the potentiation of these values leads to high scattering at higher voltages. Authors discard all data that is within 25% of the highest calculated values ending up with 90% of total data to smooth the remaining values to investigate trends of the coefficient. b) Shows a zoom-in on the values, and the considered ones colored in gray. The smoothed diffusion coefficient curve increases to a sharp peak at 2.88 V before decreasing rapidly to a minimum at 3 V. Two more minima at 3.6 and 3.7 V can be identified with small peaks in between. The voltages of the minima also fit the peak voltages for phase transition, lithiation but also the additional peaks found in the dQ/dV analysis.

The remaining values were smoothed to investigate trends of the coefficient and are presented in Figure 7b. The plot displays the included data (gray) and a subset of the excluded data (blue). Distinct peaks at 2.88 V, around 3.48, 3.65, 3.84, and 4.15 V can be identified, with respective minima around 3.1, 3.6, 3.7, 3.88 V, and a declining trend beyond 4.15 V. The voltages of the minima coincide the peak voltages for phase transition, lithiation but also the additional peaks found in the dQ/dV analysis and are reasonable to also influence diffusion. The 3.1 V is wide and could be assigned to the 3.2 V formation peak even though it was not visible in the dQ/dV plot. The structural changes of the phase transitions lead to more intercalation sides and less favorable sides become accessible at higher voltages but is limited to the maximum number of sides and therefore decreases again before reaching maximum.

Figure 8 presents the respective results for all cells and formation strategies. Most cells show similar transients of the pseudodiffusion coefficient which seems plausible. Elevated peak heights are observed for extended current durations, particularly in the double length and pulsed 5s formation. The authors are aware of the different hights being the reason also of the fits and other calculations and therefore renounce from an explanation for now.

To the best of the authors knowledge there is no existing data of the diffusion coefficient trajectory over the formation process but the coefficients of a regular cycle dependent on the state of charge measured by Nikiforidis et al.[27] at least also shows peaks and minima throughout the measurement.
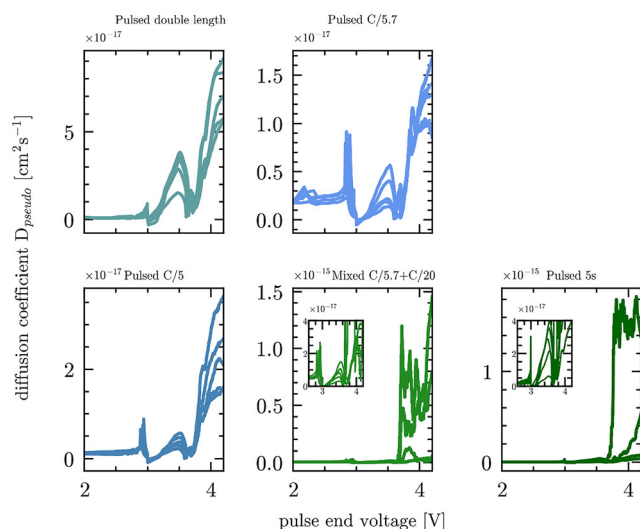
Batteries & Supercaps

Research Article
doi.org/10.1002/batt.202500153

Chemistry Europe
European Chemical
Societies Publishing

Figure 8. Calculated pseudodiffusion coefficient of all five cells of each formation strategy filtered the same way as described before. For most of the cells the peaks identified previously for one C/5.7 cell can be found and the transient matches. Higher peaks can be found for the double length and C/5.7 cells.

4. Summary and Conclusion

Potential in situ analyses of ICA, HPPC, and GITT were conducted for pulsed formation to extract the quality-indicating parameters of differential capacity (dQ/dV), IR, and a pseudodiffusion coefficient. All dQ/dV peaks corresponding to phase transitions observed during conventional constant-current formation were also identifiable in the pulsed formation protocol, regardless of pulse shape. The transient behavior of IR remains open for discussion due to the lack of comparable literature, while the resistance values at 4 V are consistent with those later obtained via HPPC.

A pseudodiffusion coefficient based on the Weppner–Huggins approach was derived. For the square root fit for $dE/d\sqrt{t}$, a composite fitting function was employed to enhance the fit quality, particularly around voltages associated with phase transitions. The square root component is presumed to describe the diffusion-limited behavior, whereas the exponential term may account for first-order kinetic reactions. In the case of $dE/d\delta$, the stoichiometric change δ was assumed constant due to the small magnitude of the pulses, and the voltage relaxation during the rest period was fitted with an exponential function to determine the OCV. The voltage change ΔE per pulse was then defined as the difference in OCVs. After filtering out unrealistic values attributable to the limited voltage resolution, a meaningful trend emerged that aligned well with the reactions identified through the dQ/dV analysis. It is important to note that the evaluation of the pseudodiffusion coefficient is inherently more complex due to the required assumptions and the fitting strategies employed.

Acknowledgments

Conflict of Interest

Among others, L.M., B.Z., and H.S.S. are named inventors on a related patent application published under WO2024170596 with the title "METHOD AND DEVICE FOR FORMING AN ELECTROCHEMICAL DEVICE"[18] and may benefit through Arbeitnehmererfindergesetz ArbnErfG, specifically §40. Patenting rights are owned by Karlsruher Institut für Technologie.

Data Availability Statement

Please refer to Reference 10 for Data Availability and Specifics.

[1] D. L. Wood, J. Li, S. J. An, *Joule* **2019**, *3*, 2884.
[2] H. H. Heimes, A. Kampker, C. Lienemann, M. Locke, C. Offermanns, S. Michaelis, E. Rahimzei, *Lithium-ion Battery Cell Production Process*, PEM der RWTH Aachen University, DVMA, Aachen, Frankfurt am Main **2018**.
[3] H. H. Heimes, C. Offermanns, A. Mohsseni, H. Laufen, U. Westerhoff, L. Hoffmann, P. Niehoff, M. Kurrat, M. Winter, A. Kampker, *Energy Technol.* **2020**, *8*, 1900118.
[4] G. Garcia, E. Ventosa, W. Schuhmann, *ACS Appl. Mater. Interfaces* **2017**, *9*, 18691.
[5] G. García, S. Dieckhöfer, W. Schuhmann, E. Ventosa, *J. Mater. Chem. A Mater.* **2018**, *6*, 4746.
[6] K.-F. Ren, H. Liu, J. X. Guo, X. Sun, C. Guo, W. Bao, F. Yu, X. B. Cheng, J. Li, *ChemSusChem* **2025**, *18*, e202401401.
[7] K. Cicvarić, S. Pohlmann, B. Zhang, F. Rahmanian, L. Merker, M. Gaberšček, H. S. Stein, *Phys. Chem. Chem. Phys.* **2024**, *26*, 14713.
[8] F.-M. Wang, H.-Y. Wang, M.-H. Yu, Y.-J. Hsiao, Y. Tsai, *J. Power Sources* **2011**, *196*, 10395.
[9] S. Zhu, C. Hu, Y. Xu, Y. Jin, J. Shui, *J. Energy Chem.* **2020**, *46*, 208.
[10] L. Merker, M. Blessing, B. Zhang, H. S. Stein, *Adv. Intel. Discov.* **2011**, 202500025, https://doi.org/10.26434/chemrxiv-2025-9zf4v.
[11] S. J. An, J. Li, Z. Du, C. Daniel, D. L. Wood, *J. Power Sources* **2017**, *342*, 846.
[12] T. S. Pathan, M. Rashid, M. Walker, W. D. Widanage, E. Kendrick, *J. Phys. Energy* **2019**, *1*, 44003.
[13] P.-C. J. Chiang, M.-S. Wu, J.-C. Lin, *Electrochem. Solid-State Lett.* **2005**, *8*, A423.
[14] R. Drees, F. Lienesch, M. Kurrat, *J. Energy Storage* **2021**, *36*, 102345.
[15] H.-H. Lee, Y.-Y. Wang, C.-C. Wan, M.-H. Yang, H.-C. Wu, D.-T. Shieh, *J. Power Sources* **2004**, *134*, 118.
[16] X. Cui, S. D. Kang, S. Wang, J. A. Rose, H. Lian, A. Geslin, S. B. Torrisi, M. Z. Bazant, S. Sun, W. C. Chueh, *Joule* **2024**, *8*, 3072.
[17] Z. Fei, F. Yang, K.-L. Tsui, L. Li, Z. Zhang, *Energy* **2021**, *225*, 120205.
[18] L. H. Rieger, E. Flores, K. F. Nielsen, P. Norby, E. Ayerbe, O. Winther, T. Vegge, A. Bhowmik, *Digit. Discovery* **2023**, *2*, 112.

Batteries & Supercaps

Research Article
doi.org/10.1002/batt.202500153

Chemistry Europe
European Chemical
Societies Publishing

[19] M. Yang, X. Sun, R. Liu, L. Wang, F. Zhao, X. Mei, *Appl. Energy* **2024**, *376*, 124171.

[20] X. Qu, D. Shi, J. Zhao, M.-K. Tran, Z. Wang, M. Fowler, Y. Lian, A. F. Burke, *J. Energy Chem.* **2024**, *94*, 716.

[21] M. Dubarry, B. Y. Liaw, *J. Power Sources* **2009**, *194*, 541.

[22] Y. Li, M. Abdel-Monem, R. Gopalakrishnan, M. Berecibar, E. Nanini-Maury, N. Omar, P. van den Bossche, J. van Mierlo, *J. Power Sources* **2018**, *373*, 40.

[23] Y. Chen, L. Torres-Castro, K.-H. Chen, D. Penley, J. Lamb, M. Karulkar, N. P. Dasgupta, *J. Power Sources* **2022**, *539*, 231601.

[24] I. Landa-Medrano, A. Eguia-Barrio, S. Sananes-Israel, S. Lijó-Pando, I. Boyano, F. Alcaide, I. Urdampilleta, I. de Meatza, *J. Electrochem. Soc.* **2020**, *167*, 90528.

[25] M. J. Lacey, *ChemElectroChem* **2017**, *4*, 1997.

[26] A. Weng, P. Mohtat, P. M. Attia, V. Sulzer, S. Lee, G. Less, A. Stefanopoulou, *Joule* **2021**, *5*, 2971.

[27] G. Nikiforidis, M. Raghibi, A. Sayegh, M. Anouti, *J. Phys. Chem. Lett.* **2021**, *12*, 1911.

[28] M. Jia, W. Zhang, X. Cai, X. Zhan, L. Hou, C. Yuan, Z. Guo, *J. Power Sources* **2022**, *543*, 231843.

[29] S. D. Kang, W. C. Chueh, *J. Electrochem. Soc.* **2021**, *168*, 120504.